PHYSICAL REVIEW B **89**, 184409 (2014)

Magnetic structures of non-cerium analogues of heavy-fermion Ce_2RhIn_8: The case of Nd_2RhIn_8, Dy_2RhIn_8, and Er_2RhIn_8

Petr Čermák,[1,2,*] Pavel Javorský,[2] Marie Kratochvílová,[2] Karel Pajskr,[2] Milan Klicpera,[2] Bachir Ouladdiaf,[3] Marie-Hélène Lemée-Cailleau,[3] Juan Rodriguez-Carvajal,[3] and Martin Boehm[3]

[1]*Jülich Centre for Neutron Science JCNS, Forschungszentrum Jülich GmbH, Outstation at MLZ, Lichtenbergstraße 1, 85747 Garching, Germany*

[2]*Charles University, Faculty of Mathematics and Physics, Department of Condensed Matter Physics, Ke Karlovu 5, 121 16 Prague 2, The Czech Republic*

[3]*Institut Laue Langevin, 6 rue Jules Horowitz, BP156, 38042 Grenoble Cedex 9, France*

(Received 18 March 2014; revised manuscript received 25 April 2014; published 15 May 2014)

R_2RhIn_8 compounds (space group $P4/mmm$, R is a rare-earth element) belong to a large group of structurally related tetragonal materials which involves several heavy-fermion superconductors based on Ce. We have succeeded in growing single crystals of compounds with Nd, Dy, and Er, and following our previous bulk measurements, we performed neutron-diffraction studies to determine their magnetic structures. The Laue diffraction experiment showed that the antiferromagnetic order below the Néel temperature is in all three compounds characterized by the propagation vector $\mathbf{k} = (1/2,1/2,1/2)$. The amplitude and direction of the magnetic moments, as well as the invariance symmetry of the magnetic structure, were determined by subsequent experiments using two- and four-circle diffractometers. The critical exponents were determined from the temperature dependence of the intensities below T_N.

DOI: 10.1103/PhysRevB.89.184409 PACS number(s): 75.25.−j, 61.05.fg, 61.05.fm

I. INTRODUCTION

The group of heavy-fermion tetragonal compounds based on the $CeIn_3$ common structural unit became important after the discovery of a superconducting state under applied pressure in $CeRhIn_5$ [1] and later at ambient pressure in $CeCoIn_5$ [2], $CeIrIn_5$ [3], and recently Ce_2PdIn_8 [4]. This family of structurally related compounds, generally written as $Ce_nT_mIn_{3n+2m}$ (where T is a transition metal element Co, Rh, Ir, Pd, or Pt, and n and m are integers), consists of n layers of $CeIn_3$ alternating along the c axis with m layers of TIn_2. The possibility of changing the dimensionality in these materials by varying the m and n together with changing of the T element gives scientists a big playground for tuning the ground state properties of these compounds (see Ref. [5]). Since the discovery of similarities between the heavy-fermion superconductivity and the ^{3}He magnetic superfluid state, it is believed that these phenomena are mediated by a nearly localized Fermi liquid state and thus, with a magnetic origin [6]. Hence, a detailed investigation of the magnetic interactions in these materials is of importance to understand their unconventional superconductivity.

The simplest crystal structure in this family of materials forms the cubic $CeIn_3$ ($m = 0$ and $n = 1$), where cerium atoms are arranged with a fully 3D character ("13" structure). $CeIn_3$ orders antiferromagnetically (AF) at $T_N = 10$ K with propagation vector $\mathbf{k} = (1/2, 1/2, 1/2)$ [7]. By adding a layer of TIn_2 after every second $CeIn_3$ layer, one can obtain the so-called "218" structure ($n = 2$, $m = 1$), where layers of Ce atoms start to interact quasi-two-dimensionally. The only AF ordered cerium compound with the "218" structure is Ce_2RhIn_8 showing AF transition at $T_N = 2.8$ K, while other compounds undergo a transition to superconducting state or exhibit a non-Fermi liquid behavior. Ce_2RhIn_8 orders magnetically with the commensurate (C) propagation $\mathbf{k} = (1/2, 1/2, 0)$ and a staggered cerium moment of 0.55 μ_B pointing 52° out of the ab plane [8]. The stacking of cerium moments within the ab plane remains the same as in $CeIn_3$, but moments stop propagating along the tetragonal c axis.

Adding one layer of TIn_2 between neighborhood cerium planes leads to a complete disappearance of the original cubic cell and to a formation of the so-called "115" structure ($m = n = 1$). The arrangement of Ce atoms in this type of structure reveals stronger 2D character compared to the 218 structure. The interest has mainly focused on the 115 compounds in the past years, as they reveal higher superconducting temperatures. Moreover, their synthesis does not suffer from inclusions and stacking faults as it is often observed in 218 single crystals. Magnetic order at ambient pressure was found in $CeRhIn_5$ below $T_N = 3.8$ K. It exhibits similar properties as its 218 analog, but it forms incommensurate (IC) AF structure propagating with a wave vector $\mathbf{k} = (1/2, 1/2, 0.297)$ and cerium magnetic moments of 0.75 μ_B lying within the ab plane [9,10]. The amplitude of the moment constitutes the major part of a value expected from the crystal-field calculations (0.92 μ_B) [11] which speaks for 4f-localized magnetism. Influence of neighboring Ce layers is decreased leading to IC propagation along the c axis. The other existing compounds of the cerium 115 family (T = Co, Ir) become superconducting at low temperatures and do not exhibit magnetic order without applied magnetic field. By applying an external magnetic field along the crystallographic $[1\bar{1}0]$ direction in $CeCoIn_5$, the so-called Q phase appears with magnetic moments of 0.15 μ_B aligned along the c axis and propagating with the wave vector $\mathbf{k} = (0.45, 0.45, 1/2)$ [12]. It is questionable whether this magnetic ordering has its origin in the so-called FFLO phase or not, see Ref. [5] and references therein. The latest study by Raymond *et al.* [13] showed the

*cermak@mag.mff.cuni.cz

possibility of inducing the same Q phase by a small amount of neodymium doping, raising again the question of the origin of such magnetic ordering.

The recently discovered compound $CePt_2In_7$ ("127" structure, $m = 2$ and $n = 1$) enhances the 2D character of these compounds: layers of cerium are alternating with two layers of TIn_2. $CePt_2In_7$ orders antiferromagnetically below 5.4 K [14]. Coexistence of commensurate $\mathbf{k} = (1/2, 1/2, 1/4)$ and incommensurate $\mathbf{k} = (1/2, 1/2, \delta)$ magnetic structures was revealed by NMR measurement [15]. The incommensurate component vanishes under pressure and, simultaneously, superconductivity emerges. However the exact magnetic order remains unknown.

Latest studies on the $CeIn_3$ based systems showed the possibility to grow structures with even more exotic stacking "3-1-11" or "5-2-19" [16,17]. Especially the first mentioned structure seems very promising for further study, as the compound Ce_3PdIn_{11} exhibits two magnetic ($T_1 = 1.63$ K, $T_N = 1.49$ K) transitions and a superconducting transition ($T_c = 0.42$ K) at ambient pressure [18]. Details of its magnetic structure remain unknown.

In summary, magnetic structures in cerium-based compounds embody a complex behavior resulting from a mixing of competing effects. To understand magnetic interactions in these compounds, it is useful to follow the evolution of their magnetic structures as a function of different rare-earth elements. The binary RIn_3 alloys belong to the most studied systems. In contrast to $CeIn_3$, they all have magnetic ground state with a propagation vector $\mathbf{k} = (1/2, 1/2, 0)$. The amplitudes and directions of magnetic moments in the ground state are summarized in Table I. The majority of RIn_3 compounds exhibits a succession of different magnetic phases with decreasing temperature, resulting in a simple commensurate ground state structure. For example the magnetic phase diagram of $NdIn_3$ includes two incommensurate phases in zero magnetic field [19].

The majority of non-cerium "115" and "218" compounds orders AF and can be split into four groups according to the direction of the easy magnetization axis. Generally, compounds with $R = Pr$ remains paramagnetic (except Pr_2PdIn_8 [20]), compounds $R =$ Gd and Sm are nearly isotropic, compounds with $R =$ Nd, Tb, Dy, Ho have the easy magnetization axis along the tetragonal c axis, and the easy magnetization axis lies within the ab plane in the case of compounds with Er and Tm reflecting the crystal-field anisotropy. As shown in Table I, only a limited number of "218" and "115" magnetic structures have been studied microscopically. Compounds containing Ga on positions of In atoms form the same structure for heavy rare-earth atoms (Gd-Yb) [21]. These intermetallics have similar bulk properties as their indium relatives. Magnetic structures were determined on $TbCoGa_5$ and R_2CoGa_8 ($R =$ Gd-Tm). All these non-cerium compounds are usually influenced by the RKKY interaction, crystalline electrical field (CEF) effects, and the hybridization between 4f-electrons and conduction electrons [22,23].

In this paper we report the determination of the magnetic structures of R_2RhIn_8 (with $R =$ Nd, Dy, and Er) compounds using the single crystal neutron diffraction technique. As the Pr compound from this family exhibits a nonmagnetic singlet ground state [38], the Nd-based compound is the natural candidate that should be primarily investigated. Moving along the lanthanide series, we have chosen Dy and Er based compounds for a detailed study. Dy_2RhIn_8 represents a typical member of heavy rare-earth compounds, having the same direction of the easy magnetization axis as Nd_2RhIn_8 [39] but a much larger amplitude of the ordered magnetic moments [40]. Both neodymium and dysprosium based compounds exhibit very sharp steps in magnetization curves indicating the existence of a field-induced phase in their magnetic phase diagram [40]. Similar phase diagrams were reported for their 115 relatives [41], cobalt-galium relatives [42], and Tb_2RhIn_8 [40], pointing to a similar magnetic scenario. On the other hand, Er_2RhIn_8 represents a compound where the easy magnetization axis lies within the ab plane. Rather smooth steps in the magnetization curves were observed in this case when applying a field along the twofold [110] direction [40]. In total, bulk properties of all three studied compounds are similar to the structurally related $RRhIn_5$ [43] and R_2CoGa_8 [42] compounds.

In order to determine the magnetic structure in these materials, we have performed two types of neutron diffraction experiments. First, neutron Laue diffraction images were taken to explore the reciprocal space and find the propagation vectors. Subsequently standard two- or four-circle diffraction experiments were carried out to determine the magnetic structures in detail.

II. EXPERIMENT

Single crystals of Nd_2RhIn_8, Dy_2RhIn_8, and Er_2RhIn_8 were prepared by the solution growth method from an indium flux [44]. The elements with starting compositions 2:1:40, 2:1:30, and 2:1:50, respectively, were put into alumina crucibles, sealed under high vacuum and heated up to 910 °C. The mixture was then slowly cooled down to 400 °C where the remaining indium solution was centrifuged. In this way we obtained plate-shaped cuboid single crystals. The samples selected for further macroscopic and microscopic measurements were of sizes about $1.7 \times 1.5 \times 0.8$ mm^3, $2.5 \times 0.4 \times 0.4$ mm^3, and $4 \times 1.5 \times 0.2$ mm^3, respectively. The c axis was always oriented perpendicular to the plate. The chemical composition and homogeneity were verified by an energy-dispersive x-ray detector Bruker AXS and the tetragonal space group $P4/mmm$ together with lattice parameters were confirmed on single crystal x-ray RIGAKU RAPID II diffractometer. Atomic positions of R_2RhIn_8 are presented in Table II.

Neutron Laue diffraction experiments on Nd_2RhIn_8 and Dy_2RhIn_8 crystals were performed on the VIVALDI instrument at Institute Laue Langevin (ILL), Grenoble [45]. The Laue patterns were recorded in the paramagnetic state at 30 and 40 K, respectively, and in the ordered state at 2 K. In order to maximize the number of observed reflections and to discover any possible purely magnetic intensities, the crystal was mounted with obvious symmetry axes well away from the vertical axis. Nine patterns at 10 degree intervals of rotation about the vertical axis were taken at each temperature. Each pattern was exposed for 115 minutes. The propagation vector of the Er_2RhIn_8 was determined on the CYCLOPS

TABLE I. Known magnetic structures at ambient pressure and zero magnetic field for $R_nT_m\mathrm{In}_{3n+2m}$ and $R_nT_m\mathrm{Ga}_{3n+2m}$ compounds.

Compound	**k** vector	Direction[a]	Amplitude (μ_B)	T_N (K)	
		"13"			
$CeIn_3$ (Ref. [7])	(1/2, 1/2, 1/2)		0.48	10	[b]
$NdIn_3$ (Ref. [19])	(1/2, 1/2, 0)	*c* axis	2	5.9	[c]
$GdIn_3$ (Ref. [24])	(1/2, 1/2, 0)	*c* axis		44	
$TbIn_3$ (Ref. [25])	(1/2, 1/2, 0)	10°	8.4	32	
$DyIn_3$ (Ref. [26])	(1/2, 1/2, 0)	27°	8.8	24	
$HoIn_3$ (Ref. [25])	(1/2, 1/2, 0)	58°	9	7.9	
$ErIn_3$ (Ref. [27])	(1/2, 1/2, 0)	[111]		4.8	
$TmIn_3$ (Ref. [28])	(1/2, 1/2, 0)	[111]	4.89	1.6	[d]
		"115"			
$CeRhIn_5$ (Refs. [9,10])	(1/2, 1/2, 0.297)	*ab* plane	0.75	3.8	
$CeCoIn_5$ (Ref. [12])	(0.44, 0.44, 1/2)	*c* axis	0.15	0.3	[e]
$Ce_{0.95}Nd_{0.05}CoIn_5$ (Ref. [13])	(0.45, 0.45, 1/2)			0.9	
$NdRhIn_5$ (Ref. [29])	(1/2, 0, 1/2)	*c* axis	2.5	11	
$GdRhIn_5$ (Ref. [30])	(1/2, 0, 1/2)	*b* axis		39	
$TbRhIn_5$ (Ref. [31])	(1/2, 0, 1/2)	*c* axis	9.5	47.3	
$DyRhIn_5$ (Ref. [32])	(1/2, 0, 1/2)	*c* axis	8.1	28.1	
$HoRhIn_5$ (Ref. [32])	(1/2, 0, 1/2)	*c* axis	7.6	15.8	
$TbCoGa_5$ (Ref. [33])	(1/2, 0, 1/2)	*c* axis		36.2	[f]
$HoCoGa_5$ (Ref. [34])	(1/2, 0, 1/2)	*c* axis		9.6	[g]
		"218"			
Ce_2RhIn_8 (Ref. [8])	(1/2, 1/2, 0)	38°[h]	0.55	2.8	
Tb_2RhIn_8 (Ref. [35])	(1/2, 1/2, 1/2)	[i]		42.8	
Gd_2IrIn_8 (Ref. [36])	(1/2, 0, 0)	*ab* plane[h]		40.8	
Sm_2IrIn_8 (Ref. [37])	(1/2, 0, 0)	*ab* plane[h]		14.2	[j]
Gd_2CoGa_8 (Ref. [23])	(1/2, 1/2, 1/2)	*ab* plane[k]		20.0	
Tb_2CoGa_8 (Ref. [23])	(1/2, 1/2, 1/2)	*c* axis[k]		28.5	
Dy_2CoGa_8 (Ref. [23])	(1/2, 1/2, 1/2)	*c* axis[k]		15.2	
Ho_2CoGa_8 (Ref. [22])	(1/2, 1/2, 1/2)	*c* axis		5.1	
Er_2CoGa_8 (Ref. [21])	(0, 1/2, 0)	*a* axis[h]	4.71	3.0	
Tm_2CoGa_8 (Ref. [21])	(1/2, 0, 1/2)	*a* axis[k]	2.35	2.0	

[a]Value in degrees means inclination from the *c* axis.
[b]Magnetic moment direction cannot be determined by neutron diffraction.
[c]This C structure is stabilized below 4.7 K. Above this temperature there is a mixture of IC phases.
[d]Compound also contains $\mathbf{k} = (0, 0, 1/2)$ propagation and an IC component.
[e]In the magnetic field 11 T applied along the $[1\bar{1}0]$ direction.
[f]Magnetic structure for the phase between 5.4 and 36.2 K.
[g]This C structure is stabilized below 7.5 K. Between this temperature and T_N exists an IC phase with $\mathbf{k} = (0.5, 0, 0.35(2))$.
[h]$+-+-$ stacking along the *c* axis.
[i]$+--+$ stacking along the *c* axis.
[j]Direction of the moments was determined to be 18° from the *a* axis.
[k]$++--$ stacking along the *c* axis.

instrument also at ILL [46]. Laue patterns were collected in the paramagnetic (8 K) and in the antiferromagnetic (1.5 K) state. 26 patterns (each exposed for 15 minutes) at 5 degree intervals were taken at each temperature. A series of Laue patterns with changing temperature were also taken in order to reveal possible phase transitions. All Laue patterns, both from the VIVALDI and the CYCLOPS instruments, were indexed and integrated using the Esmeralda Laue Suite software [47].

TABLE II. Atomic Positions of $R_2\mathrm{RhIn}_8$, space group *P4/mmm*

Atom		*x*	*y*	*z*
R	2g	0	0	*z*(*R*)
Rh	1b	0	0	1/2
In1	2f	1/2	0	0
In2	4i	1/2	0	*z*(In2)
In3	2h	1/2	1/2	*z*(In3)

The four-circle neutron diffraction experiments were performed for the Nd and Dy samples on the D10 diffractometer at ILL, with a wavelength $\lambda = 2.36$ Å using pyrolytic graphite monochromator and filter before the sample. The reflections were measured as ω scans. After cooling the samples to 2 K, cell parameters and orientation were refined on the basis of 41 (Nd) and 20 (Dy) strong nuclear reflections using the program RAFD9 [48]. Then a set of reflections at 2 K and temperature dependencies of selected magnetic and nuclear

TABLE III. Summary of performed single crystal diffraction experiments

	Nd_2RhIn_8	Dy_2RhIn_8	Er_2RhIn_8
instrument	D10	D10	IN3
absorbtion coefficient (cm^{-1})	9.018	19.134	10.707
number of measured reflections (nonequivalent)			
nuclear	364 (70)	350 (68)	60 (21)
magnetic	461 (50)	383 (38)	57 (15)

reflections were measured. All reflections were integrated and corrected for Lorentz factor using the program RACER [49].

In the case of Er_2RhIn_8, we have used the triple axis spectrometer IN3 at ILL. We measured the reflections in the elastic condition at $\lambda = 2.36$ Å using ω scans as well. The sample was mounted with the [110] and the [001] lattice vectors in the scattering plane. After cooling to 1.5 K, the tilt of the sample was adjusted by a goniometer and lattice parameters were refined. Contrary to D10, IN3 has only ^{3}He detector tube. All measured data sets were fitted with Gaussian profiles, and the integrated intensities were corrected for the Lorentz factor.

Moreover, the integrated intensities of all reflections were corrected for absorption in the crystal using Gaussian grid integration [50] with the program DATAP [51]. Used absorption coefficients together with the number of measured reflections are listed in Table III. The obtained raw data were reduced using the program DataRed [52]. The program FullProf [52] was used for the refinement of the nuclear and magnetic structures. The extinction correction was refined using the Zachariasen formula [53] with anisotropic correction (Ext − Model = 4 in FullProf software).

III. RESULTS AND DISCUSSION

The specific heat of Nd_2RhIn_8 was measured to compare the magnetic characteristics of our sample with previously published data [39]. The C_p vs T dependence (see Fig. 1) shows a well pronounced λ-type anomaly corresponding to the magnetic phase transition. The ordering temperature $T_N = (10.8 \pm 0.1)$ K can be deduced from our data, in good agreement with the previously published value of $T_N = 10.7$ K [55]. Also the measured absolute values and the magnetic entropy (not shown here), determined after subtraction of specific heat of La_2RhIn_8 taken from Ref. [54], correspond well to the values reported by Pagliuso [55]. As the specific heat does not show any sign of a further phase transition down to 2 K, we expect a single magnetic phase in zero magnetic field. Similar conclusions can be made for dysprosium and erbium compounds, based on our previous measurements performed on the same piece of single crystals [40].

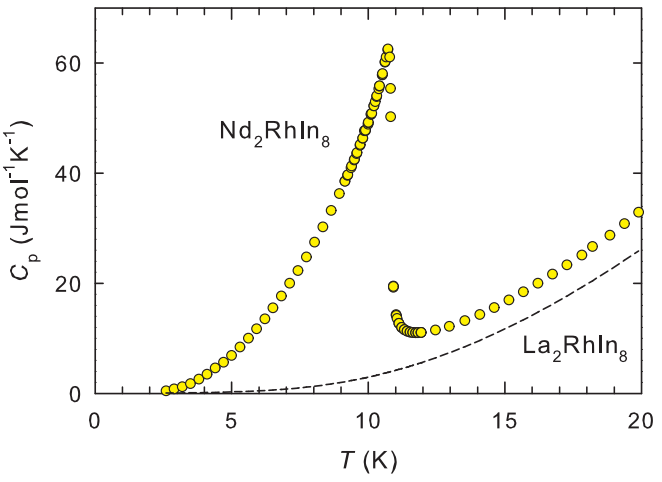

FIG. 1. (Color online) Specific heat of Nd_2RhIn_8. The dashed line shows the specific heat of a nonmagnetic analog La_2RhIn_8 (Ref. [54]).

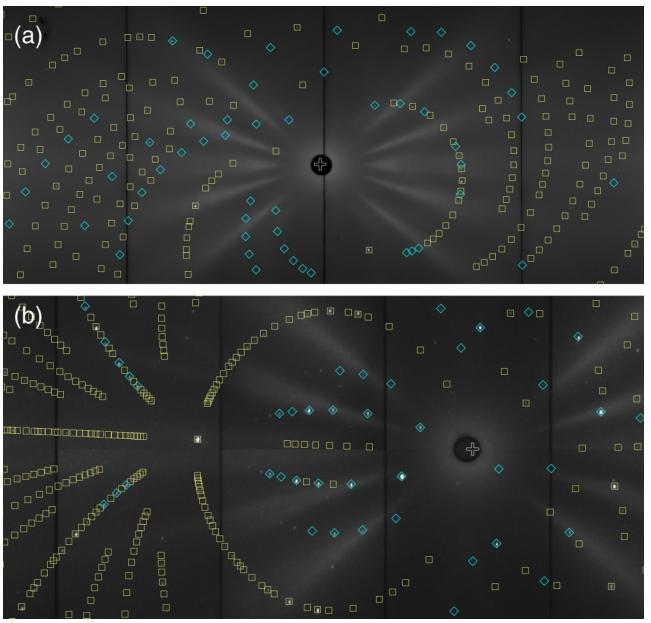

FIG. 2. (Color online) Laue picture of (a) Nd_2RhIn_8, (b) Er_2RhIn_8 taken at 2 and 1.5 K, respectively. Yellow squares denote nuclear reflections while blue diamonds denote magnetic ones. The diffuse streaks correspond to the textured powder pattern due to Al in the cryostat.

The overall Laue patterns for Nd_2RhIn_8 and Er_2RhIn_8 are represented in Fig. 2. All the observed diffraction spots at paramagnetic temperature can be indexed assuming the tetragonal structure with the space group $P4/mmm$. At the cryostat base temperature, a large number of new, purely magnetic reflections, appear. All magnetic reflections in all three compounds can be described by a single propagation vector $\mathbf{k} = (1/2, 1/2, 1/2)$. To illustrate this observation, we show a smaller cut of the Laue picture of Nd_2RhIn_8 in Fig. 3. The intensities along the [001] crystallographic direction, indicated in Fig. 3(b), are then shown in Fig. 4. The knowledge of the propagation vector was subsequently used during the further single crystal diffraction experiments. The structural parameters at the lowest temperature are summarized in Table IV, and the observed vs calculated integrated nuclear intensities are depicted in Fig. 5.

The temperature dependence of selected nuclear intensities of Nd_2RhIn_8 and Dy_2RhIn_8 is shown in Fig. 6. We observed no change in intensity above and below the transition temperature,

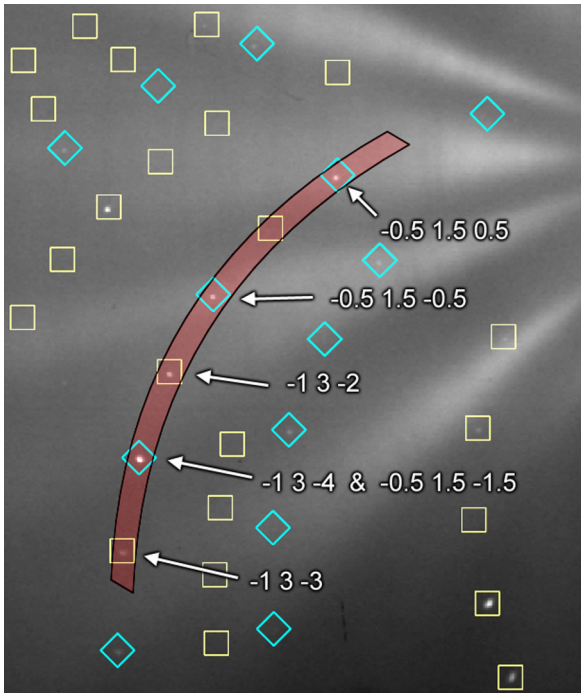

FIG. 3. (Color online) Part of the Laue picture of Nd_2RhIn_8 with diffraction spots marked as in Fig. 2. Red color denotes area of integration along the reciprocal $[hkl]^*$ (with $h = -1$, $k = 3$, and $l = n$) direction which corresponds to the intensities shown in Fig. 4.

indicating that there is no contribution with a $\mathbf{k} = (0, 0, 0)$ propagation vector. A similar conclusion can be deduced from the temperature dependence of Laue patterns from CYCLOPS (not shown) for Er_2RhIn_8, where no change in nuclear intensities is observed as well.

In order to restrict the number of possible magnetic structures, we applied symmetry arguments as developed in the representation analysis [56]. The different irreducible

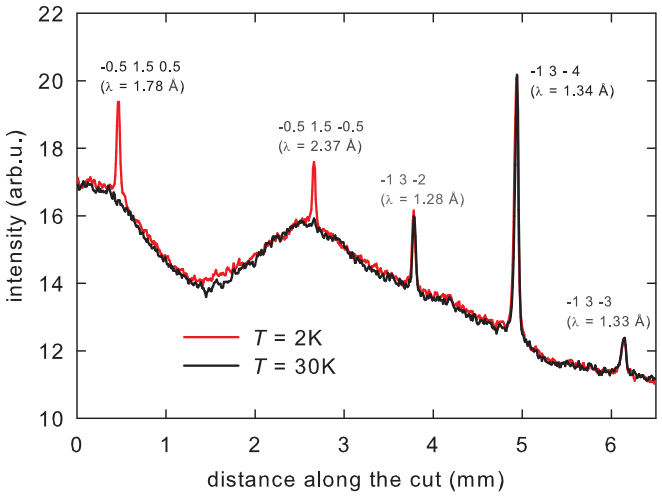

FIG. 4. (Color online) Diffraction intensities taken from a cut through a Laue picture of Nd_2RhIn_8 as indicated in Fig. 3(b). Note that individual positions could correspond simultaneously to several reflections that are overlapped with different wavelengths.

TABLE IV. Structural and magnetic parameters of R_2RhIn_8 at $T = 2$ K.

R	Nd	Dy	Er
lattice parameters			
a (Å)	4.6213(9)	4.572(2)	4.552(2)
c (Å)	12.113(3)	11.96(1)	11.980(2)
atomic positions along the c axis			
R	0.3083(3)	0.3095(2)	0.311(1)
In(2)	0.3059(6)	0.3078(7)	0.311(1)
In(3)	0.1212(4)	0.1226(5)	0.125(2)
magnetic structure			
$\mathbf{k}$	(1/2, 1/2, 1/2)		
μ (μ_B)	2.53(9)	6.9(3)	6.4(1.4)
direction	c axis	c axis	ab plane
c stacking	$++--$	$++--$	$++--$
T_N (K)	10.63(4)	24.24(8)	3.70(6)
β	0.22(3)	0.20(1)	0.16(2)
reliability factors			
nuclear RF^2	6.70	5.58	11.8
nuclear RF	5.34	4.40	9.94
nuclear χ^2	3.14	2.58	3.57
magnetic RF^2	15.5	9.46	20.2
magnetic RF	9.83	6.95	13.2
magnetic χ^2	6.01	2.65	8.29

representations with their associated basis vectors have been calculated with the help of the BasIreps program [52] using the previously measured propagation vector $\mathbf{k} = (1/2, 1/2, 1/2)$. The little group (or group of the propagation vector) coincides with the space group $G_\mathbf{k} = P4/mmm$ (all rotational symmetry operators of $P4/mmm$ leave invariant the propagation vector), so the small representations coincide with the full irreducible representations of the space group. There are together 10 irreducible representations (*irreps*) associated with the $\mathbf{k} = (1/2, 1/2, 1/2)$ propagation vector. Two of them, Γ_9 and Γ_{10}, are two dimensional, and the remaining eight are one dimensional. However, the global reducible magnetic representation of the R 2g site can be decomposed in *irreps* as $\Gamma_{2g} = \Gamma_2 + \Gamma_7 + \Gamma_9 + \Gamma_{10}$. Because there are always two magnetic sublattices corresponding to the 2g Wyckoff site within the unit cell, the basis vectors have six components each. The first three correspond to the magnetic moment components of the R atom at the position with x,y,z site symmetry (R1) and the other three to those of the atom at the $-x,y,-z+1$ site (R2). By making linear combinations of the basis vectors within the same irreducible representation, we obtain the vectors representing the components of the magnetic moments of both atoms. These combinations are summarized in Table V. One can see that in the case of the one-dimensional representations Γ_2 and Γ_7 there is only a single free parameter u describing the magnetic structure. For the two-dimensional representations Γ_9 and Γ_{10}, there are, in general, two parameters u and v. In both cases the difference between Γ_2 and Γ_7, or Γ_9 and Γ_{10}, respectively, resides in either the parallel or antiparallel coupling between the two rare-earth sublattices. As the propagation vector is $\mathbf{k} = (1/2, 1/2, 1/2)$, the magnetic unit cell is doubled in the x,y,z direction, and the

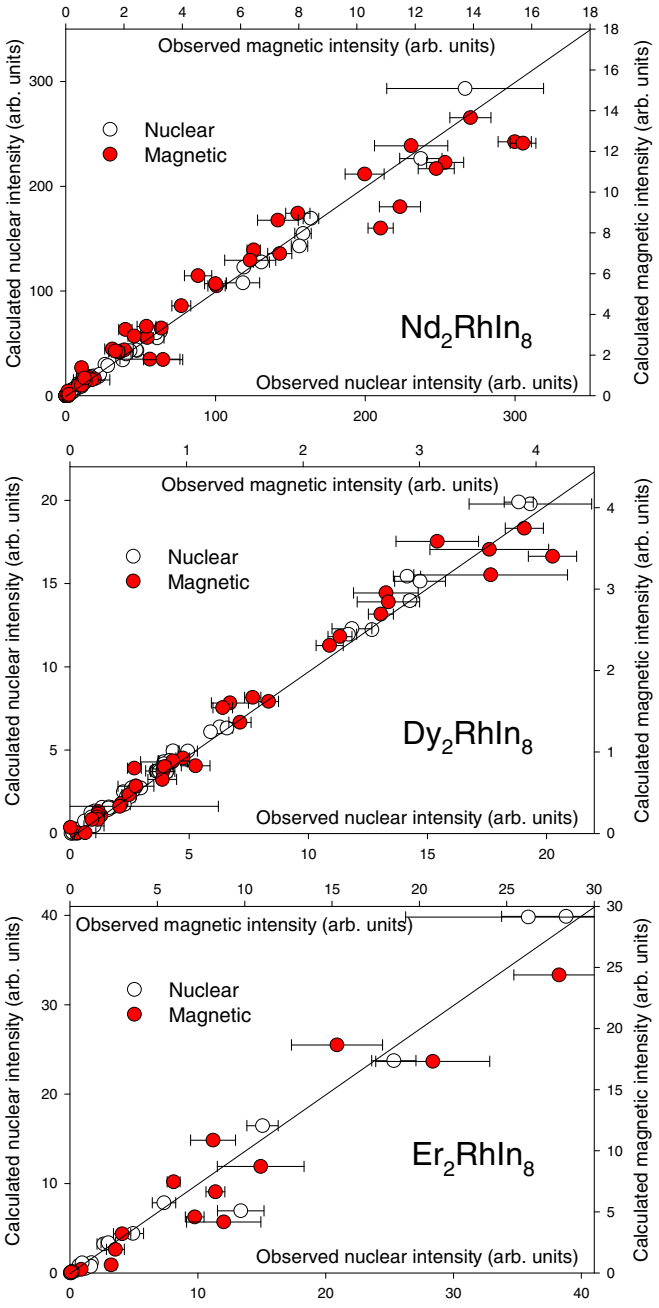

FIG. 5. (Color online) Observed and calculated integrated nuclear and magnetic intensities. The calculated intensities correspond to the parameters given in Table IV. Arbitrary units are used, but values for each compound are scaled together with the same ratio.

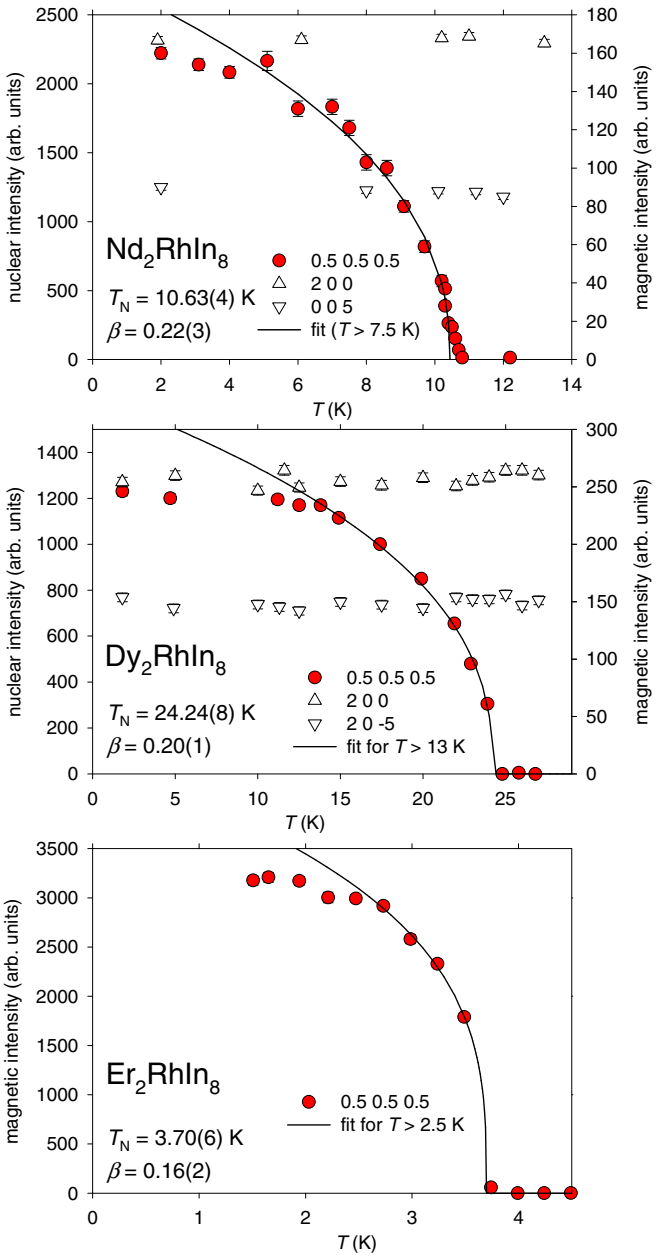

FIG. 6. (Color online) Temperature dependence of intensities of selected reflections. The full line is a fit to Eq. (1).

direction of the moments in the neighboring (chemical) unit cells have to be opposite.

From the point of view of the invariance symmetry of the spin configurations described by the above representations, it is easy to determine the Shubnikov groups for all of them using tools like the Bilbao Crystallographic Server [57,58] or the suite of programs existing in the ISOTROPY site [59]. In the case of 1D *irreps* Γ_2 and Γ_7 the Shubnikov group is tetragonal and the same: I_c4/mcm in BNS notation, or $P_I4/mm'm'$ in OG notation, except that the z coordinate of the R1 atom is different for the two *irreps*. For the 2D *irreps* we have more possibilities because we can select different directions in the representation space. These directions correspond to particular values of u and v. The direction $(a,0)$ corresponds to $v = 0$, and the direction $(0,b)$ corresponds to $u = 0$, and all

TABLE V. Direction of magnetic moments for all possible irreducible representations corresponding to the propagation wave vector $\mathbf{k} = (1/2, 1/2, 1/2)$ and the magnetic 2g site in the $P4/mmm$ space group.

Site	Γ_2	Γ_7	Γ_9	Γ_{10}
R1	$0\,0\,u$	$0\,0\,u$	$u\,-v\,0$	$u\,v\,0$
R2	$0\,0\,-u$	$0\,0\,u$	$-u\,v\,0$	$u\,v\,0$

of them gives rise to the same orthorhombic Shubnikov group for both 2D *irreps* Γ_9 and Γ_{10}: $F_S mmm$ in BNS notation, or $P_I mmm$ in OG notation, with different atom positions for each representation and direction. For the direction (a,a) we have $u = v$ and the symmetry is also orthorhombic: $I_b mma$ in BNS notation, or $C_I m'mm$ in OG notation for both 2D *irreps*. A general direction in the representation space correspond to different values of u and v and lowers the symmetry to monoclinic: $C_a 2/m$ in BNS notation or $P_C 2/m$ in OG notation for both 2D *irreps*. The differences for each *irrep* correspond always to different positions of the magnetic atoms in the standard setting of the Shubnikov group. The combination of two *irreps*, like $\Gamma_2 + \Gamma_9$, lowers still the symmetry to triclinic in the general case.

A good agreement between observed and calculated intensities of Nd_2RhIn_8 and Dy_2RhIn_8 is obtained for magnetic moments pointing along the c axis with their parallel alignment within one unit cell and corresponding to Γ_2. For Er_2RhIn_8 the fitting procedure showed that the far best agreement is obtained with the model Γ_{10} where the magnetic moments in the unit cell lie in the ab plane pointing the same direction. For Er_2RhIn_8 only reflections within the (-110) scattering plane could be measured, which were not sufficient to determine the exact direction of the moments within the ab plane.

The obtained magnetic structures are depicted in Fig. 7. The refined moments are summarized in Table IV. The comparison of observed and calculated intensities for all compounds is shown in Fig. 5. For completion of the magnetic refinement the rare-earth moments were allowed to lie in a general direction by combining two representations in order to check a lowering of symmetry. We did not observe any noticeable improvement of the fits, and the local minima were always found within 1–2 degrees out of the previously determined direction using a single representation. We can therefore conclude that the magnetic moments of Nd_2RhIn_8 and Dy_2RhIn_8 lie along the tetragonal c axis, maintaining the tetragonal symmetry in the group $P_I 4/mm'm'$, while they lie within the ab plane in the case of Er_2RhIn_8, lowering the symmetry at least to orthorhombic (remember that for experimental limitations we could not determine the directions of the moment within the ab plane).

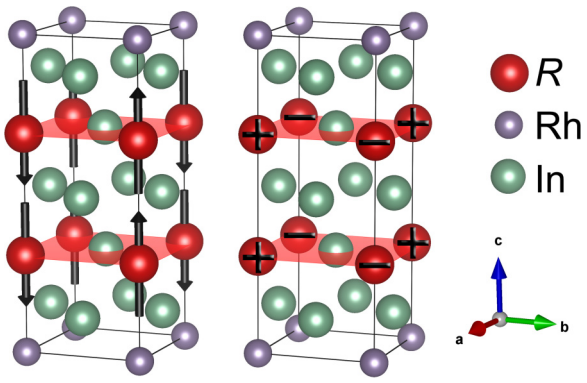

FIG. 7. (Color online) Magnetic structure of (a) Nd_2RhIn_8 and Dy_2RhIn_8, (b) Er_2RhIn_8 compounds. Note that magnetic moments of Er_2RhIn_8 can point anywhere within the ab plane, but are all parallel to each other.

The temperature dependence of the intensity of the (1/2, 1/2, 1/2) magnetic reflection for each compound is shown in Fig. 6. The data were fitted to the power law

$$I \propto (T_N - T)^{2\beta}. \quad (1)$$

The determined transition temperatures T_N as well as the critical exponents β are listed in Table IV. These experimental results are compatible neither with Ising prediction for the two-dimensional ($\beta = 0.125$) and the three-dimensional ($\beta = 0.313$) systems nor with the X-Y ($\beta = 0.345$) or Heisenberg ($\beta = 0.367$) models. However, all three compounds reveal qualitatively similar critical behavior pointing to the similar ordering mechanism with the value of $\beta \sim 0.2$. We are aware that the determined critical exponents are fitted from the temperature ranges down to 0.8 of the reduced temperature T/T_N, which could also explain the deviation from the theoretical values. The small value of $\beta = 0.16$ for Er_2RhIn_8 is rather different from the value $\beta = 0.33$ determined for isostructural Er_2CoGa_8 [21]. We observe a significantly steeper increase of the spontaneous magnetization compared to the gallium-based compound, although both materials share a similar magnetic structure.

Let us now compare our results with the magnetic structures in related compounds in terms of dimensionality. As mentioned in the introduction, the "218" compounds can be seen as transition from the nearly two-dimensional "115" towards the three-dimensional "13" compounds. In the neodymium compounds the different "13" and "115" magnetic structures were ascribed to competing ($NdIn_3$) or matching ($NdRhIn_5$) crystal-field and exchange anisotropies [29]. The magnetic moments in both Nd_2RhIn_8 and $NdRhIn_5$ point along the c axis, driven by the crystal-field anisotropy. The coupling between the neighboring Nd moments is antiferromagnetic within the basal planes, although the moments propagate differently: $\mathbf{k}_{\text{in-plane}} = (1/2, 1/2)$ in Nd_2RhIn_8 and $\mathbf{k}_{\text{in-plane}} = (1/2, 0)$ in $NdRhIn_5$. The $NdIn_3$ layer (in $NdRhIn_5$) or bilayer (in Nd_2RhIn_8) is then separated by a $RhIn_2$ layer. The Nd-Nd coupling along the c axis across this nonmagnetic layer is in both cases also antiferromagnetic. The coupling along the c axis within the cubic $NdIn_3$ blocks in Nd_2RhIn_8 is ferromagnetic, i.e., these cubic blocks form the same magnetic structure occurring in the ground state of $NdIn_3$. The magnetic structure can be viewed also in the following way: among the two nearest Nd layers it acts exactly as in $NdIn_3$ (diagonal propagation in the plane perpendicular to the moments) while another Nd bilayer, separated by $RhIn_2$ layer, is coupled antiferromagnetically creating the overall propagation vector $\mathbf{k} = (1/2, 1/2, 1/2)$.

Similar conclusions are valid for dysprosium compounds, except the fact that in the cubic $DyIn_3$ the magnetic moments point out of the main crystallographic directions. A recently studied gallium analog of the dysprosium compound, Dy_2CoGa_8, shows the same magnetic structure and stacking along the c axis [23]. Stacking of moments along the c axis $++--$ in Nd_2RhIn_8 and Dy_2RhIn_8 is different from the stacking $+-+-$ revealed for Tb_2RhIn_8 [35]. This is then reflected in the qualitatively different magnetization curves in magnetic fields above 10 T applied along the a axis [60].

No magnetic structure is reported for any of the erbium 115 compounds. We can compare our results to the gallium analog Er_2CoGa_8, which has $\mathbf{k} = (0, 1/2, 0)$, i.e. it propagates only along the direction of the magnetic moments with $+-+-$ stacking along the c axis. This qualitative change of stacking within the unit cell as well as different propagation vector is probably caused by the smaller distance between Er atoms in the gallium compound (4.2287 Å in Er_2CoGa_8 [21] compared to 4.5284 Å in Er_2RhIn_8). The determined amplitude of the magnetic moment in the gallium compound 4.7 μ_B is also significantly reduced in comparison with 6.4 μ_B for its indium relative.

In all three compounds the amplitude of the ordered moments is reduced from the expected values of the free ion, in agreement with other compounds from the series [21,32]. This is typical for tetragonal CEF driven magnetic structures [61], for example $DyCo_2Si_2$ [62]. Interpolating the measured magnetization curves along the c axis to zero magnetic field for Nd_2RhIn_8 and Dy_2RhIn_8 gives the values of 2.2 and 7.2 μ_B per R atom, respectively [40,60], which are in good agreement with our experimental values. Doing the same for Er_2RhIn_8 leads to the value of 7.8 μ_B per Er for the magnetic field applied along the [110] direction and to the value of 6.9 μ_B per Er for the magnetic field applied along the [100] direction [40]. From the determined Shubnikov groups it is clear that *irrep* Γ_{10} is always connected with lowering of the symmetry and creation of the magnetic domains. That is the reason why values from bulk magnetization measurements are bigger than the value of 6.4 μ_B obtained from the neutron diffraction.

The magnetic structures in the corresponding cerium compounds are more complex. An incommensurate spiral structure, with Ce moments within the ab planes, is observed in $CeRhIn_5$ [9]. The magnetic structure of Ce_2RhIn_8 is described by the propagation vector $\mathbf{k} = (1/2, 1/2, 0)$ and Ce moments pointing 38° out of the tetragonal c axis. The coupling within the basal planes is the same as in Nd_2RhIn_8, but the coupling along the c axis is different: It is antiferromagnetic across the nonmagnetic $RhIn_2$ layer as well as within the cubic $CeIn_3$ blocks. The main difference is however the moment direction. Thus, the resulting structure lowers the symmetry by mixing two representations within the same exchange multiplet [63]. We assume that this is the consequence of stronger isotropic exchange interactions with respect to the anisotropy in the Ce compound.

IV. CONCLUSION

We have determined the magnetic structure of three intermetallic compounds, Nd_2RhIn_8, Dy_2RhIn_8, and Er_2RhIn_8, by the means of neutron diffraction experiments. All compounds are characterized by the propagation vector $\mathbf{k} = (1/2, 1/2, 1/2)$ with ferromagnetic coupling between the nearest neighboring rare-earth layers within the unit cell. The magnetic moment direction reflects the crystal-field anisotropy in these compounds. The magnetic moments of Nd_2RhIn_8 and Dy_2RhIn_8 lie along the c axis, while the moment of Er_2RhIn_8 lies within the ab plane, reaching values of 2.53, 6.9, and 6.4 μ_B, respectively.

ACKNOWLEDGMENTS

This work was supported by the Czech Science Foundation under Grant No. P204-13-12227S and by the Grant Agency of Charles University under Grant No. 348511. The work is a part of research project LG14037 financed by the Ministry of Education, Youth and Sports, Czech Republic. Samples were prepared in MLTL (http://mltl.eu/), which is supported within the program of Czech Research Infrastructures (Project No. LM2011025). We acknowledge also the ILL for the beam-time allocation and support during our measurement.

[1] H. Hegger, C. Petrovic, E. G. Moshopoulou, M. F. Hundley, J. L. Sarrao, Z. Fisk, and J. D. Thompson, Phys. Rev. Lett. **84**, 4986 (2000).

[2] C. Petrovic, P. G. Pagliuso, M. F. Hundley, R. Movshovich, J. L. Sarrao, J. D. Thompson, Z. Fisk, and P. Monthoux, J. Phys.: Condens. Matter **13**, L337 (2001).

[3] C. Petrovic, R. Movshovich, M. Jaime, P. G. Pagliuso, M. F. Hundley, J. L. Sarrao, Z. Fisk, and J. D. Thompson, Europhys. Lett. **53**, 354 (2001).

[4] D. Kaczorowski, D. Gnida, A. Pikul, and V. Tran, Solid State Commun. **150**, 411 (2010).

[5] J. D. Thompson and Z. Fisk, J. Phys. Soc. Jpn. **81**, 011002 (2012).

[6] H. R. Ott, H. Rudigier, T. M. Rice, K. Ueda, Z. Fisk, and J. L. Smith, Phys. Rev. Lett. **52**, 1915 (1984).

[7] A. Benoit, J. Boucherle, P. Convert, J. Flouquet, J. Palleau, and J. Schweizer, Solid State Commun. **34**, 293 (1980).

[8] A. Schenck, F. N. Gygax, T. Ueda, and Y. Onuki, Phys. Rev. B **70**, 054415 (2004).

[9] W. Bao, P. G. Pagliuso, J. L. Sarrao, J. D. Thompson, Z. Fisk, J. W. Lynn, and R. W. Erwin, Phys. Rev. B **62**, R14621 (2000).

[10] W. Bao, P. G. Pagliuso, J. L. Sarrao, J. D. Thompson, Z. Fisk, J. W. Lynn, and R. W. Erwin, Phys. Rev. B **67**, 099903(E) (2003).

[11] A. D. Christianson, J. M. Lawrence, P. G. Pagliuso, N. O. Moreno, J. L. Sarrao, J. D. Thompson, P. S. Riseborough, S. Kern, E. A. Goremychkin, and A. H. Lacerda, Phys. Rev. B **66**, 193102 (2002).

[12] M. Kenzelmann, T. Strässle, C. Niedermayer, M. Sigrist, B. Padmanabhan, M. Zolliker, A. D. Bianchi, R. Movshovich, E. D. Bauer, J. L. Sarrao, and J. D. Thompson, Science **321**, 1652 (2008).

[13] S. Raymond, S. M. Ramos, D. Aoki, G. Knebel, V. P. Mineev, and G. Lapertot, J. Phys. Soc. Jpn. **83**, 013707 (2014).

[14] E. D. Bauer, H. O. Lee, V. A. Sidorov, N. Kurita, K. Gofryk, J.-X. Zhu, F. Ronning, R. Movshovich, J. D. Thompson, and T. Park, Phys. Rev. B **81**, 180507 (2010).

[15] H. Sakai, Y. Tokunaga, S. Kambe, H.-O. Lee, V. A. Sidorov, P. H. Tobash, F. Ronning, E. D. Bauer, and J. D. Thompson, Phys. Rev. B **83**, 140408 (2011).

[16] A. Tursina, S. Nesterenko, Y. Seropegin, H. Noël, and D. Kaczorowski, J. Solid State Chem. **200**, 7 (2013).

[17] M. Kratochvilova, M. Dusek, K. Uhlirova, A. Rudajevova, J. Prokleska, B. Vondrackova, J. Custers, and V. Sechovsky, J. Crystal Growth **397**, 47 (2014).

[18] M. Kratochvilova, J. Prokleska, K. Uhlirova, M. Dusek, V. Sechovsky, and J. Custers, arXiv:1403.7010.

[19] M. Amara, R. Gal'era, P. Morin, T. Veres, and P. Burlet, J. Magn. Magn. Mater. **130**, 127 (1994).

[20] D. Kaczorowski, B. Belan, L. Sojka, and Y. Kalychak, J. Alloys Compounds **509**, 3208 (2011).

[21] R. D. Johnson, T. Frawley, P. Manuel, D. D. Khalyavin, C. Adriano, C. Giles, P. G. Pagliuso, and P. D. Hatton, Phys. Rev. B **82**, 104407 (2010).

[22] C. Adriano, C. Giles, L. Coelho, G. Faria, and P. Pagliuso, Physica B **404**, 3289 (2009).

[23] J. R. L. Mardegan, C. Adriano, R. F. C. Vescovi, G. A. Faria, P. G. Pagliuso, and C. Giles, Phys. Rev. B **89**, 115103 (2014).

[24] A. Malachias, E. Granado, R. Lora-Serrano, P. G. Pagliuso, and C. A. Pérez, Phys. Rev. B **77**, 094425 (2008).

[25] N. Nereson and G. Arnold, J. Chem. Phys. **53**, 2818 (1970).

[26] G. Arnold and N. Nereson, J. Chem. Phys. **51**, 1495 (1969).

[27] A. Czopnik, H. Madge, and B. Stalinski, Phys. Status Solidi A **107**, K151 (1988).

[28] A. Murasik, A. Czopnik, L. Keller, and T. Konter, Physica Status Solidi A **189**, R7 (2002).

[29] S. Chang, P. G. Pagliuso, W. Bao, J. S. Gardner, I. P. Swainson, J. L. Sarrao, and H. Nakotte, Phys. Rev. B **66**, 132417 (2002).

[30] E. Granado, B. Uchoa, A. Malachias, R. Lora-Serrano, P. G. Pagliuso, and H. Westfahl, Phys. Rev. B **74**, 214428 (2006).

[31] R. Lora-Serrano, C. Giles, E. Granado, D. J. Garcia, E. Miranda, O. Agüero, L. Mendonça Ferreira, J. G. S. Duque, and P. G. Pagliuso, Phys. Rev. B **74**, 214404 (2006).

[32] N. V. Hieu, Ph.D. thesis, Department of Physics, Graduate School of Science, Osaka University, Japan, 2007.

[33] Y. Tokunaga, Y. Saito, H. Sakai, S. Kambe, N. Sanada, R. Watanuki, K. Suzuki, Y. Kawasaki, and Y. Kishimoto, Phys. Rev. B **84**, 214403 (2011).

[34] R. Kobayashi, K. Kaneko, S. Wakimoto, S. Chi, N. Sanada, R. Watanuki, and K. Suzuki, J. Korean Phys. Soc. **63**, 337 (2013).

[35] R. Lora-Serrano, L. M. Ferreira, D. J. Garcia, E. Miranda, C. Giles, J. G. S. Duque, E. Granado, and P. G. Pagliuso, Physica B **384**, 326 (2006).

[36] E. Granado, P. G. Pagliuso, C. Giles, R. Lora-Serrano, F. Yokaichiya, and J. L. Sarrao, Phys. Rev. B **69**, 144411 (2004).

[37] C. Adriano, R. Lora-Serrano, C. Giles, F. de Bergevin, J. C. Lang, G. Srajer, C. Mazzoli, L. Paolasini, and P. G. Pagliuso, Phys. Rev. B **76**, 104515 (2007).

[38] N. V. Hieu, H. Shishido, A. Thamizhavel, R. Settai, S. Araki, Y. Nozue, T. D. Matsuda, Y. Haga, T. Takeuchi, H. Harima, and Y. Ónuki, J. Phys. Soc. Jpn. **74**, 3320 (2005).

[39] J. Duque, R. L. Serrano, D. Garcia, L. Bufaical, L. Ferreira, P. Pagliuso, and E. Miranda, J. Magn. Magn. Mater. **323**, 954 (2011).

[40] P. Cermak, M. Kratochvilova, K. Pajskr, and P. Javorsky, J. Phys.: Condens. Matter **24**, 206005 (2012).

[41] N. V. Hieu, H. Shishido, T. Takeuchi, A. Thamizhavel, H. Nakashima, K. Sugiyama, R. Settai, T. D. Matsuda, Y. Haga, M. Hagiwara, K. Kindo, and Y. Ōnuki, J. Phys. Soc. Jpn. **75**, 074708 (2006).

[42] D. A. Joshi, R. Nagalakshmi, S. K. Dhar, and A. Thamizhavel, Phys. Rev. B **77**, 174420 (2008).

[43] N. V. Hieu, T. Takeuchi, H. Shishido, C. Tonohiro, T. Yamada, H. Nakashima, K. Sugiyama, R. Settai, T. D. Matsuda, Y. Haga, M. Hagiwara, K. Kindo, S. Araki, Y. Nozue, and Y. Ōnuki, J. Phys. Soc. Jpn. **76**, 064702 (2007).

[44] K. Uhlířová and V. Sechovský, Int. J. Mater. Res. **100**, 1242 (2009).

[45] G. J. McIntyre, M.-H. Lemée-Cailleau, and C. Wilkinson, Physica B **385-386**, 1055 (2006).

[46] B. Ouladdiaf, J. Archer, J. R. Allibon, P. Decarpentrie, M.-H. Lemée-Cailleau, J. Rodríguez-Carvajal, A. W. Hewat, S. York, D. Brau, and G. J. McIntyre, J. Appl. Crystallography **44**, 392 (2011).

[47] J. Rodriguez-Carvajal, L. Fuentes-Montero, and P. Čermák, http://lauesuite.com/.

[48] A. Filhol, "Program for the refinement of the ub-matrix, wavelength, cell parameters and instrument zero-shifts in a single crystal diffraction experiment", See web page https://forge.epn-campus.eu/projects/sxtalsoft/repository/show/rafub.

[49] C. Wilkinson, H. Khamis, R. Stansfield, and G. McIntyre, J. Appl. Crystallogr. **21**, 471 (1988); https://forge.epn-campus.eu/projects/sxtalsoft/repository/show/racer.

[50] P. Coppens, in *Crystallographic computing: proceedings of an International Summer School held in Ottawa, 4-11 August 1969*, Scandinavian university books, edited by F. Ahmed, S. Hall, C. Huber, and I. U. of Crystallography (Munksgaard, Copenhagen, 1970).

[51] P. Coppens, https://forge.epn-campus.eu/projects/sxtalsoft/wiki/Datap.

[52] J. Rodriguez-Carvajal, Physica B **192**, 55 (1993).

[53] W. H. Zachariesen, Acta Cryst. **23**, 558 (1967).

[54] P. Čermák, M. Diviš, M. Kratochvílová, and P. Javorský, Solid State Commun. **163**, 55 (2013).

[55] P. G. Pagliuso, J. D. Thompson, M. F. Hundley, and J. L. Sarrao, Phys. Rev. B **62**, 12266 (2000).

[56] E. F. Bertaut, Acta Cryst. Section A **24**, 217 (1968).

[57] M. I. Aroyo, J. M. Perez-Mato, C. Capillas, E. Kroumova, S. Ivantchev, G. Madariaga, A. Kirov, and H. Wondratschek, Z. Krist. **221**, 15 (2006); http://www.cryst.ehu.es.

[58] M. I. Aroyo, A. Kirov, C. Capillas, J. M. Perez-Mato, and H. Wondratschek, Acta Cryst. A **62**, 115 (2006).

[59] H. T. Stokes, D. M. Hatch, and B. J. Campbell, Isotropy software suite, iso.byu.edu.

[60] P. Javorský, K. Pajskr, M. Klicpera, P. Čermák, Y. Skourski, and A. Andreev, J. Alloys Compounds **598**, 278 (2014).

[61] A. Szytula and J. Leciejewicz, *Handbook of Crystal Structures and Magnetic Properties of Rare Earth Intermetallics* (CRC Press, Boca Raton, 1994).

[62] N. Iwata, K. Honda, T. Shigeoka, Y. Hashimoto, and H. Fujii, J. Magn. Magn. Mater. **90–91**, 63 (1990).

[63] Y. Izyumov, V. Naish, and S. Petrov, J. Magn. Magn. Mater. **13**, 275 (1979).